journal

X-ray Absorption Studies of Ceria with Trivalent Dopants

Ping Li,* I-Wei Chen,*·* James E. Penner-Hahn,† and Tseng-Ying Tien*·*

Department of Materials Science and Engineering and Department of Chemistry,
University of Michigan, Ann Arbor, Michigan   48109

The local structural environments of Sc^{3+} and Gd^{3+} in ceria were studied for the first time by using EXAFS (extended X-ray absorption fine structure) and XANES (X-ray absorption near edge structure) spectroscopy. Our results indicate that Sc^{3+} in 10-mol%-Sc_2O_3-doped ceria has a 7-fold-coordinated Sc-ordered structure with two different Sc–O distances (2.13 and 2.26 Å). An octahedrally coordinated Sc–O cluster is present in 5 mol% Sc_2O_3–5 mol% Gd_2O_3–CeO_2, because of the strong scavenging effect of Sc^{3+}-ions on oxygen vacancies created by Gd^{3+}. The Gd^{3+} in this sample is largely unassociated. Sc_2O_3 (5 mol%) and Gd_2O_3 (5 or 10 mol%) form random solid solutions with CeO_2. These results are consistent with the current concept of defect structures in this structural family. [Key words: X-ray, absorption, ceria, dopants, defects.]

I. Introduction

IN THE structural study of fluorite-type oxides (ZrO_2, HfO_2, CeO_2, ThO_2, UO_2, and PuO_2), ceria with different trivalent cation dopants provides a simple model system. In addition, doped ceria is an excellent oxygen ion conductor because of its defect structure at elevated temperatures. Accordingly, a considerable amount of work has been done in recent years on trivalent oxide-doped ceria,[1–5] and a good understanding of its defect structure has been developed, particularly for dilute systems.

A unit cell of CeO_2 consists of eight small cubes containing anions at their corners, with every alternate cube having a cation at its center. Figure 1(a) shows one-half of a unit cell. When trivalent dopant cations (M^{3+}) substitute for Ce^{4+}, one oxygen-ion vacancy (V_O) is introduced for every two M^{3+} in order to compensate for the lower cation charge. For a dilute solid solution (<1 mol% dopant), an elementary picture of defect structure postulates an equal number of M_{Ce}–V_O pairs and isolated M_{Ce}, both randomly distributed spatially. This model was used to interpret quantitatively the observed variation of electrical properties with dopant concentrations,[1] and has also been found useful for understanding anelastic and dielectric relaxation peaks in several M^{3+}-doped ceria.[6,7]

Among trivalent cations, anomalous behavior has been reported for Sc^{3+} doping.[8] Specifically, the ionic conductivity of Sc^{3+}-doped ceria is much smaller than that for the other dopants (e.g., Y^{3+}, Gd^{3+}, and La^{3+}), and a low-temperature relaxation peak is observed when Sc^{3+} is present. These phenomena were explained in terms of a relatively high value of enthalpy of association for the Sc_{Ce}–V_O pair and a much smaller Sc^{3+} ionic size which tends to induce a large distortion of the surrounding oxygen ions.[6] It was further suggested that, as a

result of their stronger tendency for V_O association, unassociated Sc^{3+} ions in singly doped ceria can act as scavengers for oxygen vacancies introduced by other dopants. Some experimental evidence for such scavenging association has been reported by Gerhardt *et al.* in (Sc,Y)-codoped ceria.[6]

Despite the overall self-consistency of the defect model in the dilute solid solution range, a direct verification of the local structure around a defect or a dopant was not provided in previous studies. For more concentrated solutions, some structural information can be obtained by X-ray diffraction, if there is long-range order, or electron diffraction, if at least an intermediate-range order has developed within microdomains. Extensive defect clustering into microdomains at >10 mol% M_2O_3 doping was suggested by Tesch *et al.* based on the experimental evidence in hafnia, which also has a fluorite-type structure.[9] An attractive interaction between dopant cations and anion vacancies has been used to explain both defect clustering and the common observation, in both doped zirconia and ceria, of a decreasing ionic conductivity at increasing vacancy concentrations in the high concentration regime.[10,11] Such long-range ordered structures have been widely reported for doped zirconia and hafnia,[12–14] which typically have a large size misfit between the dopant cations (e.g., Y^{3+} and Gd^{3+}) and the host cation (i.e., Zr^{4+} and Hf^{4+}). In contrast, no definitive structural study of long-range order in any doped ceria system has been reported, presumably because of the small size misfit in the system. Indeed, even if it were available, the structural information obtained from long-range order studies would not be directly relevant for understanding dilute solutions, which have mostly randomly distributed point defects, substitutional dopant cations, and their isolated complexes without any long-range orientational or spatial order.

We wish to point out that, for understanding physical properties such as diffusion and ionic conduction, it is the local structure and short-range order that are most important.[1] X-ray absorption spectroscopy (XAS) techniques can potentially provide a useful means to probe such local atomic structure. This information is obtained by measuring X-ray absorption of a probe cation (either host or dopant), at energies near the absorption edge of the probe ion. We have undertaken a systematic study of doped ceria using XAS. As will be detailed in the paper, several distinct defect/dopant configurations, probably typical of different solid solution ranges, have been observed. Specifically, XAS results for ceria solid solutions containing Sc^{3+} and Gd^{3+} are reported for the first time in this paper. In the above, Sc^{3+} was chosen because it is a severely undersized solute cation; Gd^{3+} was chosen because it is slightly oversized. The other extreme of a severely oversized solute, such as La^{3+}, was not feasible because of the proximity of the absorption edges of La^{3+} and Ce^{4+}. These results will be compared with various models of defect structures in fluorite-type oxides.

An X-ray absorption spectrum can be divided into two distinct regions: (1) the X-ray absorption near edge structure (XANES), which is within about 50 eV of the absorption edge, contains structural information regarding the valence of the absorbing probe atom, the ligand types, and the site geometry, primarily from multiple-scattering processes, and

(a) Fluorite-type Structure   (b) C-type Structure   (c) Fluorite Solid Solution

(d) An Anion Vacancy Associated With Two Dopant Cations

(e) Ordered Octahedral Structure For Cation Dopants and Anion Vacancies

(f) Larger Dopant Cation Without Any Anion Vacancy

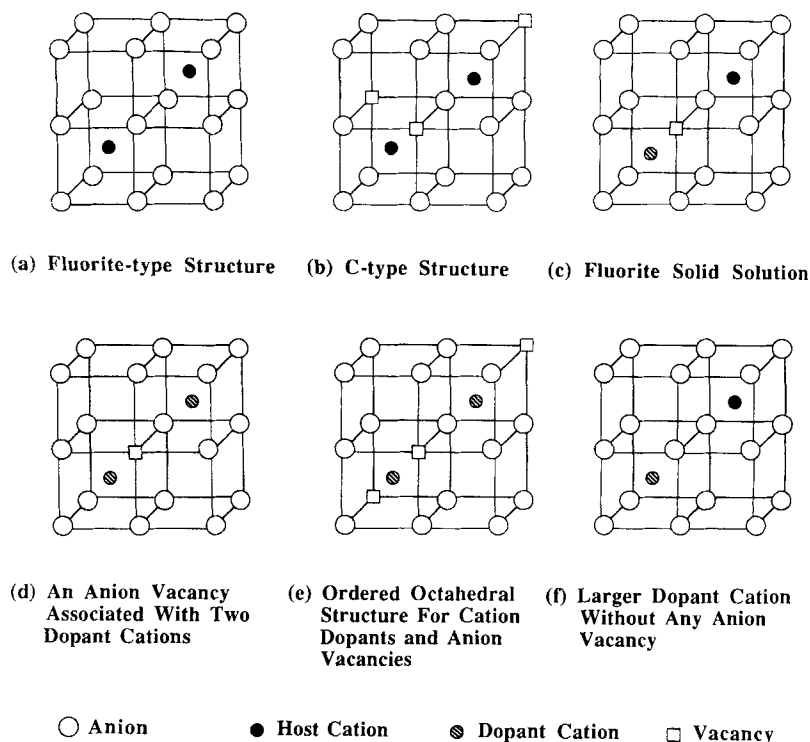○ Anion   ● Host Cation   ⊘ Dopant Cation   □ Vacancy

Fig. 1. Models illustrating various configurations of Ce, Sc, and Gd in doped Ce solid solutions: (a) CeO_2, (b) Sc_2O_3 or Gd_2O_3, (c) Sc in 5 mol% Sc_2O_3-CeO_2, (d) Sc in 10 mol% Sc_2O_3-CeO_2, (e) Sc in 5 mol% Sc_2O_3-5 mol% Gd_2O_3-CeO_2, and (f) Gd in 5 mol% Sc_2O_3-5 mol% Gd_2O_3-CeO_2.

(2) the extended X-ray absorption fine structure (EXAFS), which may extend to more than 1000 eV above the absorption edge, contains structural information regarding the interatomic distance and coordination number of the probe atom, primarily from single-scattering processes. Therefore, XANES and EXAFS are complementary probes for local structures. The analysis of the ceria structure reported here is based on both EXAFS and XANES data.

II. Experimental Procedure

(1) Powder Preparation

Ultrafine powders with a uniform composition are required for XAS measurements. Higher concentrations are preferred in order to improve the signal intensity, although formation of a second phase must be avoided. Furthermore, since the focus of the present study is placed on local structure and short-range order of cation dopants and point defects, it is desirable to avoid any significant long-range order which might obscure the picture unnecessarily. For these reasons, powders with the compositions of 1, 5, and 10 mol% M_2O_3-CeO_2 (M = Sc, In, Y, Gd, La, and Sc + Gd) were synthesized by the following method. The solutions were prepared by dissolving the dopant oxide in hot dilute HNO_3, which was mixed with the appropriate volume of cerium nitrate. High-purity powders of oxides M_2O_3 and cerium nitrate were obtained from commercial sources.[‡] Dilute NH_4OH was then added slowly to these mixed solutions, with H_2O_2 and sugar as dispersing agents, to effect coprecipitation without agglomeration. The gellike mixtures were slowly dried at 200°C and calcined at 500°C for 4 h. After hand-milling, the calcined powder samples were again oxidized in a flowing O_2 atmosphere at 850°C for 6 h to prevent the formation of Ce^{3+} ions. From our experience, the above processing temperatures and times were sufficiently low and short to avoid the precipitation of second phase and the significant development of long-range order. In this sense, although some of the

compositions had already exceeded the equilibrium solubility limit, the samples studied were in a "quenched" metastable state which was structurally similar to their more dilute counterparts.

Powders were analyzed by X-ray diffraction (XRD) with KCl as an internal standard. A high-intensity rotating anode source was used to generate $CuK\alpha$ radiation. The scan speed was usually 5°/min. Only samples which appeared to contain a single phase according to XRD were used in the subsequent XAS studies. Sc_2O_3, Gd_2O_3, and CeO_2 were also used directly as model compounds in the XAS studies.

(2) X-ray Absorption Measurements

The X-ray absorption measurements at the Ce-L_{III} edge, the Sc-K edge, and the Gd-L_{III} edge were made by using Beamline 19-A at the National Synchrotron Light Source (NSLS) under normal operating conditions (2.5 GeV, 50 to 250 mA). Energy selection was accomplished by using a double-crystal monochromator with Si(111) crystals.

XAS data for the dopant cation in 5-mol%-Sc_2O_3- or 5-mol%-Gd_2O_3-doped ceria were measured as fluorescence-excitation spectra using a large solid-angle ion chamber as the fluorescence detector. All other measurements were made in transmission mode, using ion chambers filled with N_2. Energy calibration was accomplished by placing two ion chambers behind the measured sample. A calibration standard (the oxide of the appropriate cation) was placed between them, thus allowing the absorption spectrum of the standard to be recorded at the same time as the sample spectrum. The calibration was determined by assigning the first inflection point of the standard as follows: Sc_2O_3 (4492 eV); Gd_2O_3 (7245 eV); CeO_2 (5723 eV).[15] All spectra were measured at room temperature.

Data reduction followed standard procedures for pre-edge background subtraction and EXAFS background removal.[16] The EXAFS, χ, is defined as $\chi = (\mu - \mu_s)/\mu_0$, where μ is the total absorption coefficient, μ_s is a smooth background calculated using a three-region spline, and μ_0 is the expected falloff in absorption calculated using Victoreen parameters. EXAFS data were converted to k space, $k =$

[‡]Aldrich Chemical Co., Milwaukee, WI.

$[2m(E - E_0)/\hbar^2]^{1/2}$ with E_0 assigned as 4510 eV for the Sc edge, 7270 eV for the Gd edge, and 5738 eV for the Ce edge. In the above, m is the mass of an electron, E is the photon energy, and $\hbar$ is Planck's constant divided by 2π. All Fourier transform and curve-fitting calculations were performed using k^3-weighted data.

Data were fitted to a model:[16]

$$\chi(k) = \sum_j \frac{N_j}{kR_j^2} F_j(k) \exp(-2\sigma_j^2 k^2) \sin [2kR_j + \Phi_j(k)]$$

where $F_j(k)$ is the backscattering amplitude from each of the N_j neighboring atoms of the jth type at distance R_j with a mean-square relative displacement σ_j, and $\Phi_j(k)$ is the total phase shift experienced by the photoelectron. Quantitative curve-fitting analysis utilized empirical backscattering amplitude and phase shift parameters determined from the model compounds, Sc_2O_3, Gd_2O_3, and CeO_2, for which the structural parameters (N_j, R_j, and σ_j) were known from the literature,[17] and the measured lattice parameters. The structural parameters for the solid solutions obtained from the best fit were then compared with various defect models. In the following, the results of quantitative fitting for the first nearest neighbors (i.e., cation–oxygen pairs) are analyzed. In addition, the structures of the second nearest neighbors (i.e., cation–cation pairs) are compared qualitatively using the Fourier transform of the EXAFS.

For analysis of the XANES region, the spectra were normalized as follows.[18] First, a single three-order polynomial was subtracted from the data and the resultant was then multiplied by a scale factor. The polynomial coefficients and the scale factor were chosen so as to minimize, in a least-squares sense, the deviations between the data and tabulated X-ray absorption coefficients both below and well above the edge.

It should be noted that XAS spectra are the average of scattering amplitudes of all the neighboring atoms surrounding a probe atom. Therefore, no information on the site symmetry is available. Furthermore, the coordination number, represented by N_j above, and the Debye–Waller factor, represented by σ_j above, are obviously related to each other in the data fitting procedure. They are thus inherently less definitive, rather model dependent, and should not be overinterpreted. On the other hand, the bond distance, represented by R_j, is highly accurate and can be used for qualitative comparison. The following results are presented with the above limitations in mind.

III. Results

(1) X-ray Diffraction

A linear relationship of the measured lattice parameter versus the dopant ionic radius was found (Fig. 2) for 1 and 5 mol% M_2O_3 dopants (ionic radius (Å): Ce^{4+}, 0.97; La^{3+}, 1.16; Gd^{3+}, 1.053; Y^{3+}, 1.019; In^{3+}, 0.92; and Sc^{3+}, 0.870 Å). Note that the lattice parameter for pure CeO_2 is 5.4102 Å. Thus, nearly the same lattice parameter can be achieved by Y^{3+} doping, even though Y^{3+} is slightly oversized. This can be understood by recalling that doping ceria with trivalent cations creates oxygen ion vacancies. Thus, the net variation in lattice parameter is a combination of a lattice contraction due to the formation of oxygen vacancies and a lattice expansion (contraction) due to the substitution by a larger (smaller) cation. In the case of Y^{3+} doping, the two effects nearly cancel each other, resulting in almost no distortion of the average lattice parameter.

Figure 3 shows the variation of lattice parameter with composition. At low concentrations, a linear dependence, Vegard's rule, was observed, suggesting a random solid solution of M_2O_3 in CeO_2. There are, however, two exceptions. For the 10 mol% Sc_2O_3–CeO_2 sample, the lattice constant appears to deviate from Vegard's rule. This might be indicative of the formation of some ordered distribution of the cation dopants.
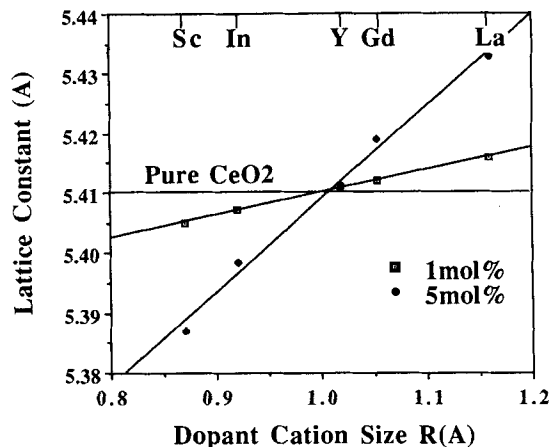
Fig. 2. Dopant size effect on lattice constant for 1-mol%- and 5-mol%-M_2O_3-doped CeO_2. M = Sc (0.87 Å), In (0.92 Å), Y (1.019 Å), Gd (1.053 Å), and La (1.16 Å). The ionic size of Ce in CeO_2 is 0.97 Å.

However, the X-ray diffraction pattern, shown in Fig. 4, did not reveal superlattice reflections. (Scandium has a much smaller scattering factor than cerium; however, even after this difference was taken into account, the amount of Sc-rich phase seems insignificant.) In addition, the lattice constant of the 5 mol% Sc_2O_3–5 mol% Gd_2O_3–CeO_2 sample is almost the same as that of pure CeO_2, and is far from the average of the lattice constants for 10 mol% Sc_2O_3–CeO_2 and 10 mol% Gd_2O_3–CeO_2, which would have been expected for a random solid solution. Once again, an ordered structure is likely to be responsible for this deviation.

(2) Sc-K Edge Measurements

The EXAFS data and the corresponding Fourier transforms (FT), for the Sc-K edge EXAFS of 5 mol% Sc_2O_3–CeO_2, 10 mol% Sc_2O_3–CeO_2, 5 mol% Sc_2O_3–5 mol% Gd_2O_3–CeO_2, and Sc_2O_3 samples, are shown in Figs. 5(a) and (b). In comparing these figures, note that the phase shift in EXAFS is carried over by Fourier transform to appear as an additive constant δ to the radial distance R in Fig. 5(b). From the FT, it is clear that the local structural environments around Sc^{3+}, an undersized cation, are distinctly different among these samples. For example, the second peak, which represents the Sc-cation shell, varies significantly from sample to sample. For 5 mol% Sc_2O_3–CeO_2 the shortest Sc-cation (Sc, Ce) distance is similar ($R + \delta \approx 3.4$ Å) to that for Ce–Ce in pure CeO_2 (see Fig. 8). This indicates that when Sc^{3+} ions substitute for Ce^{4+} ions, they are distributed randomly to
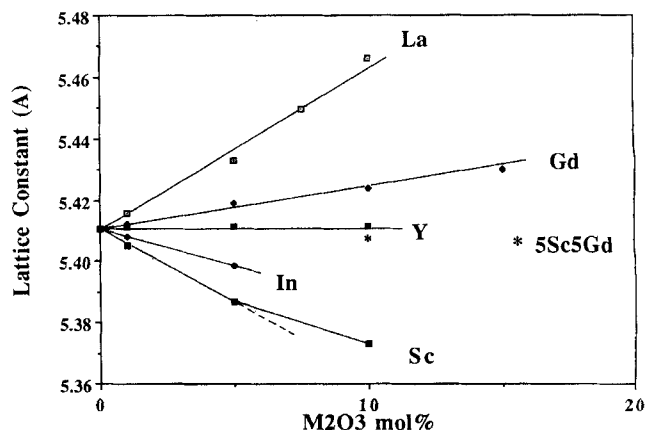
Fig. 3. Relationship between lattice constants of M_2O_3-doped ceria and dopant concentrations. Vegard's rule is observed except for 10 mol% Sc_2O_3–CeO_2 and 5 mol% Sc_2O_3–5 mol% Gd_2O_3–CeO_2.
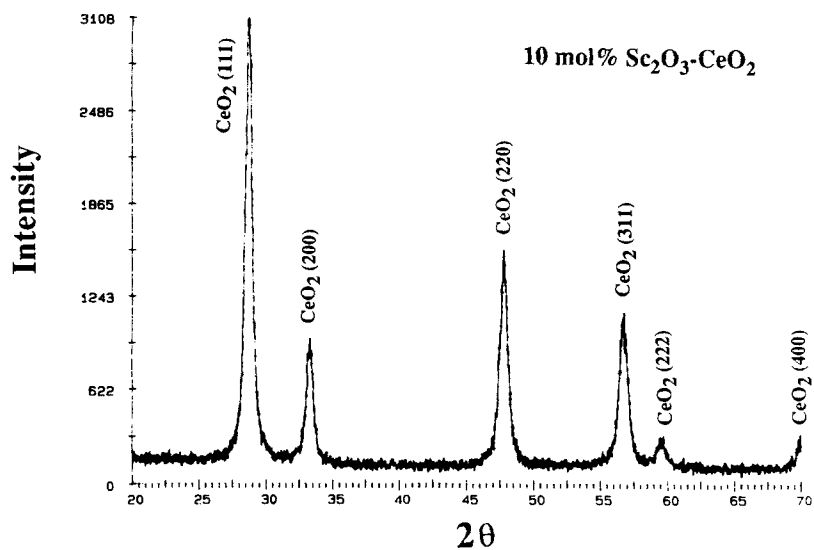
Fig. 4. X-ray diffraction pattern of 10 mol% $Sc_2O_3-CeO_2$. Only single phase ceria structure is observed.

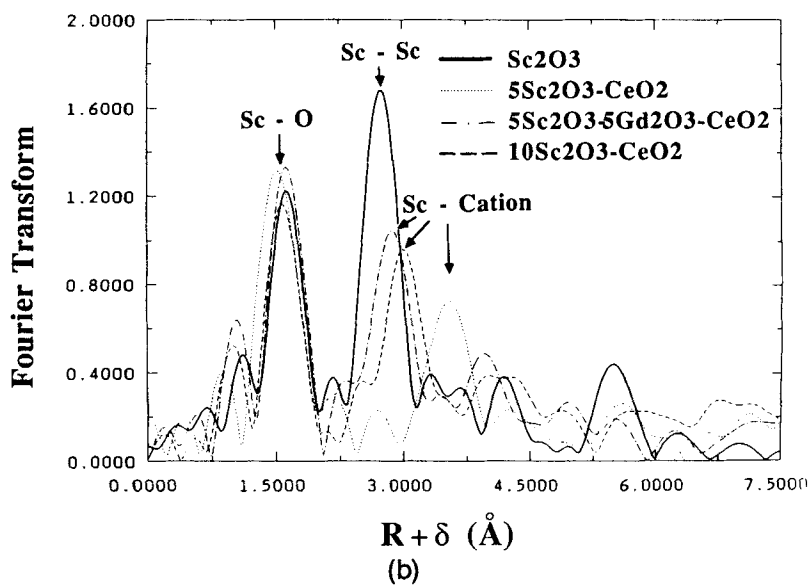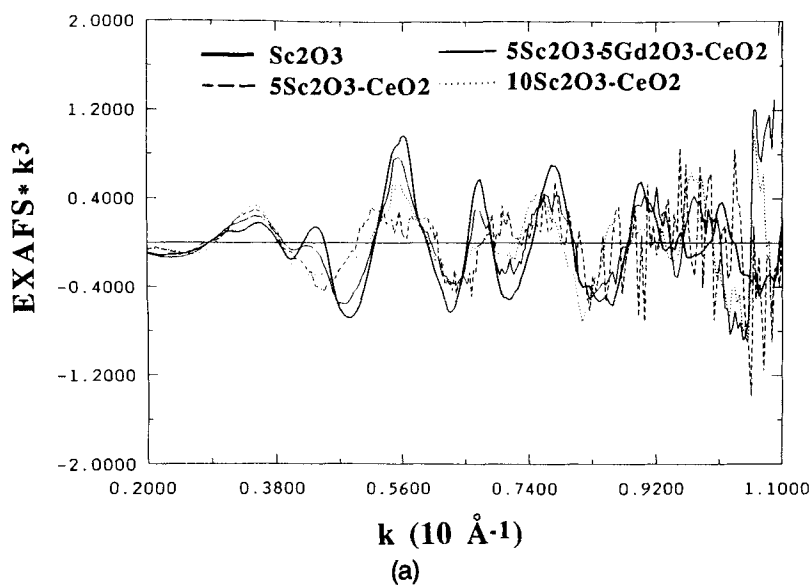**Fig. 5.** (a) k^3-weighted EXAFS from the Sc-K edge of Sc_2O_3, 5 mol% $Sc_2O_3-CeO_2$, 5 mol% Sc_2O_3–5 mol% $Gd_2O_3-CeO_2$, and 10 mol% $Sc_2O_3-CeO_2$. (b) Magnitude of the Fourier transform of data in (a) before phase shift correction (window range for k = 3 to 10.5 Å^{-1}).

form a solid solution, such as that indicated in Fig. 1(c). In contrast, the Sc-cation distance in both 10 mol% Sc_2O_3–CeO_2 and 5 mol% Sc_2O_3–5 mol% Gd_2O_3–CeO_2 is much smaller. This difference is significantly larger than would be expected as the result of change in the phase shift (δ). This suggests that Sc cations are probably clustered in both materials, which would be consistent with their smaller-than-expected lattice constants (Fig. 3).

The 5 mol% Sc_2O_3–5 mol% Gd_2O_3–CeO_2 and 10 mol% Sc_2O_3–CeO_2 samples have significantly different Sc-cation distances. Although both samples have the same total dopant concentration, the Sc-cation distance in the 5 mol% Sc_2O_3–5 mol% Gd_2O_3–CeO_2 is about 0.12 Å shorter than that in the 10 mol% Sc_2O_3–CeO_2. This occurs despite the fact that Gd^{3+} is a larger ion than Sc^{3+} and the fact that the 5 mol% Sc_2O_3–5 mol% Gd_2O_3–CeO_2 has a larger lattice constant than 10 mol% Sc_2O_3–CeO_2. Three possibilities are considered below for the ordered structure. If the Sc^{3+} and Gd^{3+} form an ordered phase together, then the Sc-cation distance should be larger when Gd^{3+} is present because of the larger Gd^{3+} ionic size. This is opposite to the experimental result. If oxygen vacancies are associated randomly with Sc^{3+} and Gd^{3+}, then both samples should have a similar Sc-cation distance, also contradicting our observation. Therefore, the most probable explanation for the shorter Sc-cation distance in Sc–Gd–CeO_2 is that the oxygen vacancies introduced by the Gd^{3+} dopant cation are associated preferentially with the clustering Sc^{3+} ions, and that they form a limited three-dimensional network with the following arrangement of ions: Sc_{Ce}–V_O–Sc_{Ce}–V_O, etc. This would lead to a 6-fold, oxygen-coordinated structure (Fig. 1(e)). Because of the constraint of the CeO_2 matrix, such a ScO_6 polyhedron should be slightly larger than the ScO_6 polyhedron in pure Sc_2O_3. (Shown in Fig. 1(b), the latter structure is commonly referred to as the C-type structure for rare-earth oxides.[20]) The Sc-cation distance is thus extended compared to the Sc–Sc distance in Sc_2O_3, as observed experimentally. To complete the comparison, we further suggest that, in 10 mol% Sc_2O_3–CeO_2, a 7-fold, oxygen-coordinated Sc ordered phase forms in a manner depicted in Fig. 1(d) so that an oxygen vacancy is shared between two Sc^{3+} (i.e., a cluster of the type Sc_{Ce}–V_O–Sc_{Ce}). This structure should have a slightly larger Sc-cation distance than the ScO_6 polyhedron in 5 mol% Sc_2O_3–5 mol% Gd_2O_3–CeO_2, which is consistent with the results in Fig. 5.

Quantitative analysis of the Sc-cation EXAFS requires Sc-cation amplitude and phase parameters. These are not readily obtainable empirically, because of the lack of good model compounds. Future work will explore the use of ab initio cal-

culations to determine the appropriate parameters. Quantitative analysis is possible, however, for the Sc–O shell by utilizing amplitude and phase parameters derived from Fourier filtered first-shell data for the appropriate oxides. The results of fitting the filtered EXAFS corresponding to the first peak in the FT are given in Table I.

In several instances, we found it necessary to use a two-shell model for the Sc–O distance to fit the data satisfactorily. Specifically, a two-shell model was significantly better than a single-shell model for fitting 5 mol% Sc_2O_3–CeO_2 and was slightly better for fitting 10 mol% Sc_2O_3–CeO_2 materials. Based on this observation, we suggest that the nominal ScO_7 polyhedron around a substitutional undersized Sc^{3+} ion is distorted, from one with equal bond lengths to one with at least two types of cation–anion distances. In doing so, the local lattice is probably distorted from a cubic type to a low symmetry type. This occurs no matter whether Sc^{3+} ions are ordered (as in 10 mol% Sc_2O_3–CeO_2) or not (as in 5 mol% Sc_2O_3–CeO_2). Further discussion of this picture will be given in the next section. In contrast to the other Sc EXAFS, no distortion is detectable in 5 mol% Sc_2O_3–5 mol% Gd_2O_3–CeO_2. The two-shell fit gives only a minor decrease in F and the two shells refine to essentially the same distance. This result is consistent with the proposal that oxygen vacancies are attracted to Sc^{3+} only, thus making the local environment of a Sc^{3+} ion in 5 mol% Sc_2O_3–5 mol% Gd_2O_3–CeO_2 a 6-fold oxygen-coordinated polyhedron. This structure would be able to relax to a regular octahedron without the need for bond distortion.

Table I also gives the fitted values of coordination number (CN) and variance in bond distance ($\Delta\sigma^2$, Debye–Waller factor). Since CN and $\Delta\sigma^2$ are highly correlated, particularly for data over a limited k range, the CN value is not particularly reliable.[16,21,22] The CN values in Table I are given for reference purposes only and we will not proceed with further interpretation of these data. It is noted that $\Delta\sigma^2$ may become negative in some cases. This means that the apparent dispersion of bond lengths in the solid solutions is smaller than that in the model compound (Sc_2O_3).

Figure 6(a) gives the Sc-K edge XANES spectra. The first derivative of XANES data from 4470 to 4530 eV is shown in Fig. 6(b). As mentioned before, XANES is sensitive to the chemical valence of the absorbing atom and the symmetry of the surrounding atoms. XANES theory, however, is not well-developed because the potential must be treated to all orders to account for multiple scattering.[23] Nevertheless, some qualitative structural information can be obtained by comparing the spectra of different samples. In Fig. 6 very different

Table I. Fitting Results of EXAFS Data

Sample	M–O	R (Å)	CN	$\Delta\sigma^2$ ($\times10^{-3}$ Å^2)	F^*
5 mol% Sc_2O_3–CeO_2	Sc–O	2.16	7.7	3.7	0.72
	Sc–O[†]	2.11	4.0[†]	−2.8	0.46
		2.28	4.0[†]	1.0	
	Ce–O	2.33	7.6	0.5	0.10
10 mol% Sc_2O_3–CeO_2	Sc–O	2.16	6.7	2.5	0.45
	Sc–O[†]	2.13	4.0[†]	−2.1	0.23
		2.26	4.0[†]	3.4	
	Ce–O	2.34	6.8	0.2	0.29
5 mol% Sc_2O_3–5 mol% Gd_2O_3–CeO_2	Sc–O	2.14	6.1	0.1	0.10
	Sc–O[†]	2.14	3.0[†]	−3.1	0.08
		2.16	3.0[†]	−2.6	
	Gd–O	2.36	6.5	2.3	0.20
	Ce–O	2.33	6.4	1.4	0.24
5 mol% Gd_2O_3–CeO_2	Gd–O	2.34	7.1	0.2	0.26
	Ce–O	2.33	7.4	0.8	0.06
10 mol% Gd_2O_3–CeO_2	Gd–O	2.33	6.9	1.7	0.24
	Ce–O	2.34	6.8	2.1	0.20

*Mean-square deviation between experimental data and calculated EXAFS. [†]Two-shell model fitting, coordination number fixed at reasonable integer values.
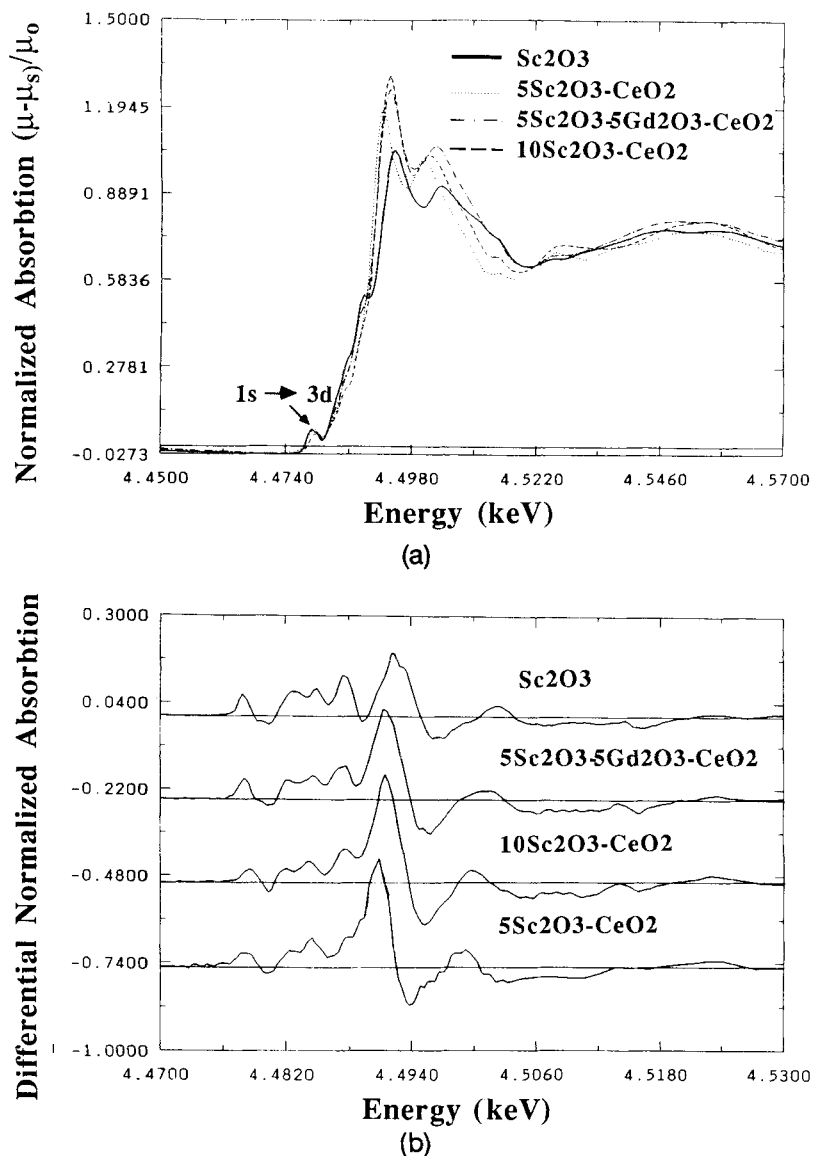
Fig. 6. (a) XANES data from Sc-*K* edge of Sc_2O_3, 5 mol% Sc_2O_3–CeO_2, 5 mol% Sc_2O_3–5 mol% Gd_2O_3–CeO_2, and 10 mol% Sc_2O_3–CeO_2. (b) First derivative of XANES data in (a).

XANES data for Sc^{3+} ion in 5 mol% Sc_2O_3–CeO_2, 10 mol% Sc_2O_3–CeO_2, 5 mol% Sc_2O_3–5 mol% Gd_2O_3–CeO_2, and Sc_2O_3 are noticeable. This, at least, means that Sc local structures are different among them. It has been established that the first peak at the lowest excitation energy is caused by the transition from the 1s-core state into the 3d state. Shoulders or kinks on the rising absorption edge have been related in the literature to the beginning of steplike continuum absorption.[23] According to this interpretation, the major discontinuity may be associated with a dipole-allowed transition resulting from a "shape resonance" of the outgoing continuum electron in the structure potential due to the ligands bound to the absorbing ion, which bears only a vague resemblance to the atomic states of isolated metal ions. However, the confining effect of the ligand cage should depend both on the bond length and on the electronegativity, or "hardness," of the confining cage. In this vein, we suggest that the strongest postedge resonance, observed in Sc_2O_3, may be correlated with the most compact and the smallest ScO_6 polyhedron in the C-type rare-earth oxide structure; that the less strong resonance of 5 mol% Sc_2O_3–5 mol% Gd_2O_3–CeO_2 probably reflects a similar but necessarily distorted ScO_6 polyhedron constrained in the ceria matrix; and, lastly, that the relatively weak resonance of 5 mol% Sc_2O_3–CeO_2 and 10 mol% Sc_2O_3–CeO_2 may be ascribed to the relatively open

geometry of the two-shell ScO_7 polyhedron which provides a lower amplitude for "trapping." (The latter is stronger than the former, probably because of the stronger confining effect of a Sc-ordered cluster in 10 mol% Sc_2O_3–CeO_2 than in the more disordered structure in 5 mol% Sc_2O_3–CeO_2.) Future theoretical modeling of these spectra in terms of their corresponding ligands is needed to confirm the above interpretation.

(3) Gd-L_{III} Edge Measurement

The k^3-weighted EXAFS from the Gd-L_{III} edge of 10 mol% Gd_2O_3–CeO_2, 5 mol% Gd_2O_3–5 mol% Sc_2O_3–CeO_2, and Gd_2O_3 and the corresponding Fourier transform are shown in Figs. 7(a) and (b). The Gd–O distances (the first peak) in the two ceria solid solutions are nearly the same as those of Gd–O in Gd_2O_3 and Ce–O in CeO_2 (Fig. 8(b)). The Gd-cation distance (the second peak) is similar to the Ce–Ce distance in CeO_2 but larger than the Gd–Gd distance in Gd_2O_3. These observations suggest that Ge^{3+} ions substitute randomly for Ce^{4+} in CeO_2. Apparently no ion ordering is occurring around the substitutional Gd^{3+} in doped ceria.

A quantitative analysis of the Gd–O shell was performed using the amplitude and phase shift obtained from the model compound Gd_2O_3. The average Gd–O distance (2.34 Å) calculated from the measured lattice parameter of C-type
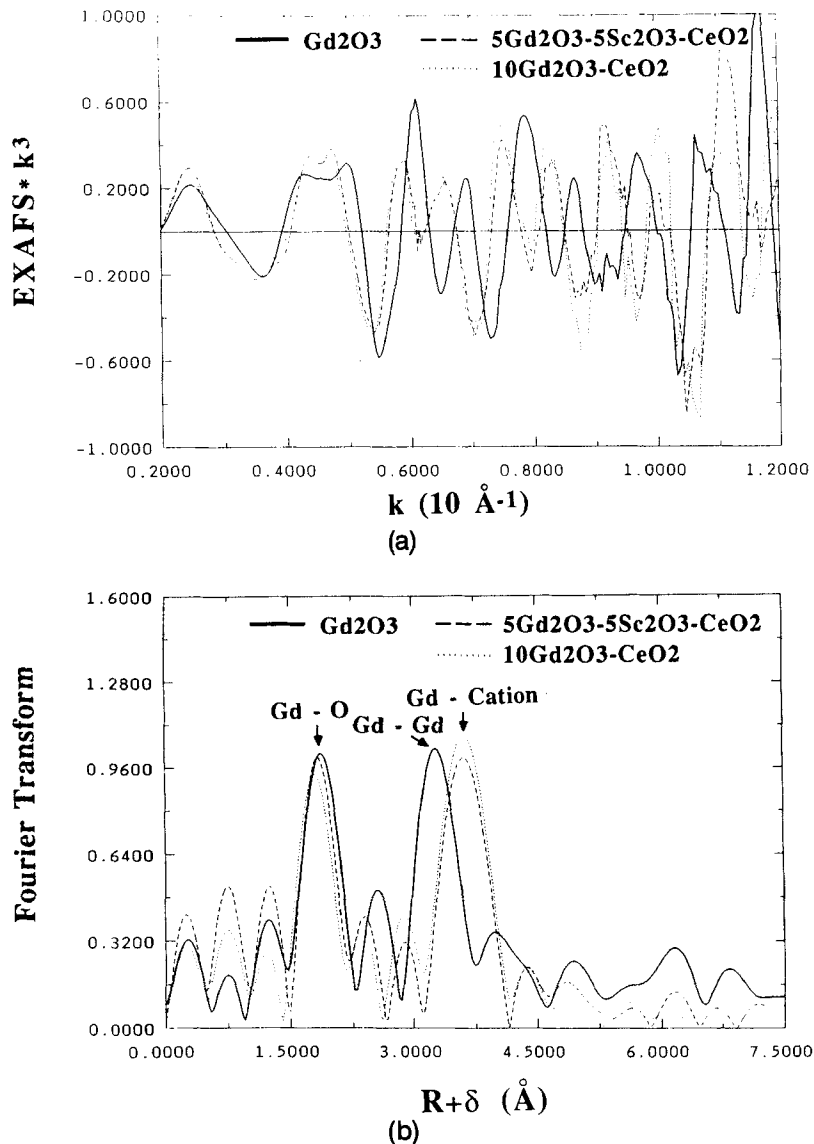
Fig. 7. (a) k^3-weighted EXAFS from the Gd-L_{III} edge of Sc_2O_3, 5 mol% Sc_2O_3–5 mol% Gd_2O_3–CeO_2, and 10 mol% Gd_2O_3–CeO_2. (b) Magnitude of the Fourier transform of data in (a) before phase shift correction (window range for k = 3 to 11 Å^{-1}).

Gd_2O_3 (Fig. 1(b)) and the oxygen coordination number, CN (6), were used in the model calculation to fit the EXAFS data of the measured samples. Curve-fitting gave the numerical values reported in Table I. They confirm that the Gd–O distances in 5 mol% Gd_2O_3–CeO_2 and 10 mol% Gd_2O_3–CeO_2 are nearly the same as those of Gd–O in Gd_2O_3 and Ce–O in CeO_2. Since Gd in Gd_2O_3 is six-fold-coordinated, and thus has a shorter bond length than expected for an 8-fold-coordinated Gd, it is likely that the CN of Gd in 5 mol% Gd_2O_3–CeO_2 and 10 mol% Gd_2O_3–CeO_2 is less than 8. The Gd–O distance in 5 mol% Gd_2O_3–5 mol% Sc_2O_3–CeO_2 is slightly larger than that in the Gd-only systems. Although the difference is only marginally significant, it may reflect the scavenging effect of Sc^{3+} on vacancies introduced by Gd^{3+} dopants, which would leave Gd^{3+} ions largely unassociated (Fig. 1(f)).

(4) Ce-L_{III} Edge Measurement

The EXAFS data for the Ce-L_{III} edge were measured for all of the samples. Representative spectra are shown in Fig. 8(a). The X-ray absorption data up to only 400 eV beyond the Ce-L_{III} edge were used for structural analysis because of the presence of the Ce-L_{II} edge at the higher energy side. Their FTs are shown in Fig. 8(b). The broader radial distribution is due to the shorter energy range available.

The FT around Ce shows no major difference in the bond lengths of Ce–O and Ce–Ce between pure ceria and the solid solutions, other than the significantly reduced EXAFS amplitudes for the latter. In general, reduced EXAFS amplitudes can result from lower coordination numbers or from a high degree of structural disorder. In our case, the smaller amplitudes of the doped ceria are probably due to the disorder of the Ce lattice caused by the dopant ions, because no major change in the average coordination number of Ce^{4+} is expected at the dopant compositions investigated. This is best illustrated by comparing the amplitude of the Ce-cation shell (the second peak in Fig. 9) at different Gd concentrations. As the Gd concentration increases, a lower amplitude corresponding to a more disordered structure is evident in Fig. 9. Similar effects will also arise from compositional disorder, i.e., the superposition of Ce–Ce and Ce–dopant EXAFS. More specifically, we can rationalize the relatively small dopant effect on the amplitude of the second peak in 10 mol% Sc_2O_3–CeO_2 by the clustering of Sc^{3+}, thus leaving Ce^{4+} relatively unperturbed. The 5 mol% Sc_2O_3–5 mol% Gd_2O_3–CeO_2 and 10 mol% Gd_2O_3–CeO_2 samples show a much larger second-shell effect, presumably because Gd^{3+} does not tend to order, and the observed EXAFS will be a mixture of Ce–Ce and Ce–Gd contributions.
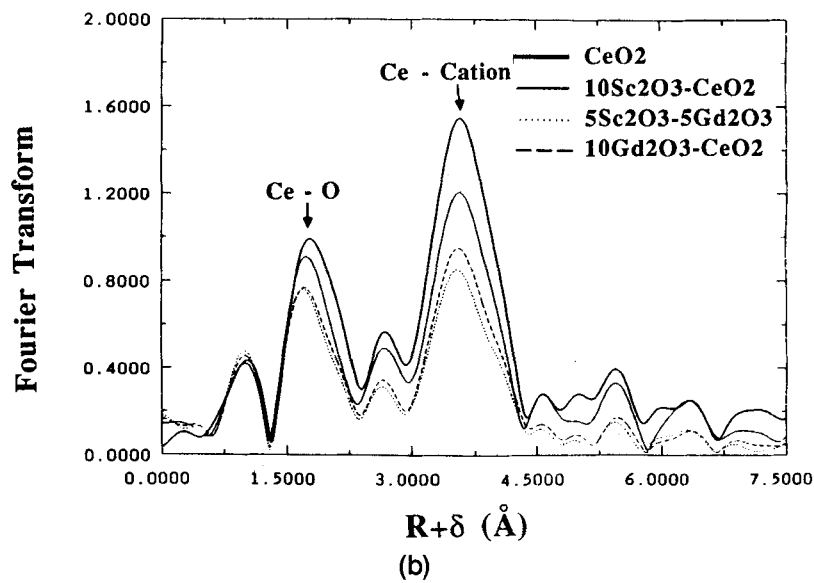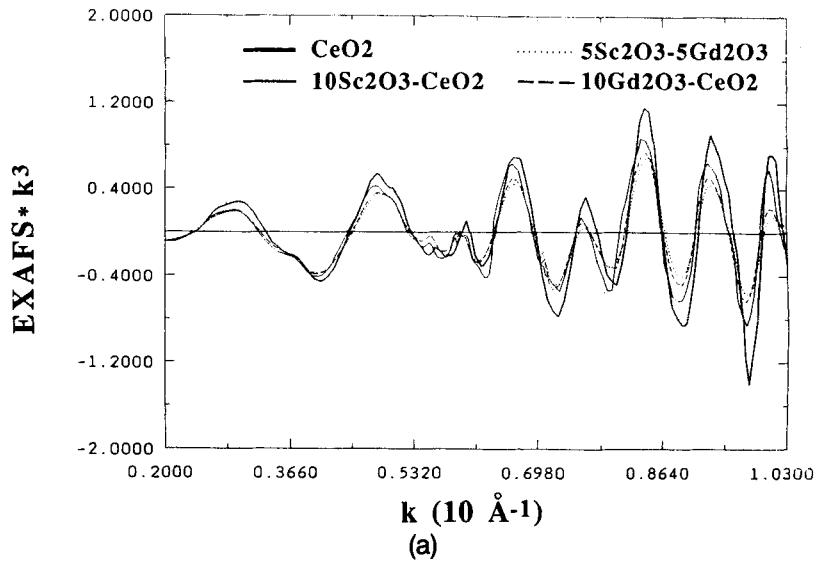
Fig. 8. (a) k^3-weighted EXAFS from the Ce-L_{III} edge Sc_2O_3, 10 mol% Sc_2O_3-CeO_2, 5 mol% Sc_2O_3-5 mol% Gd_2O_3-CeO_2, and 10 mol% Gd_2O_3-CeO_2. (b) Magnitude of Fourier transform of data in (a) before phase shift correction (window range for k = 2.8 to 10.3 Å^{-1}).
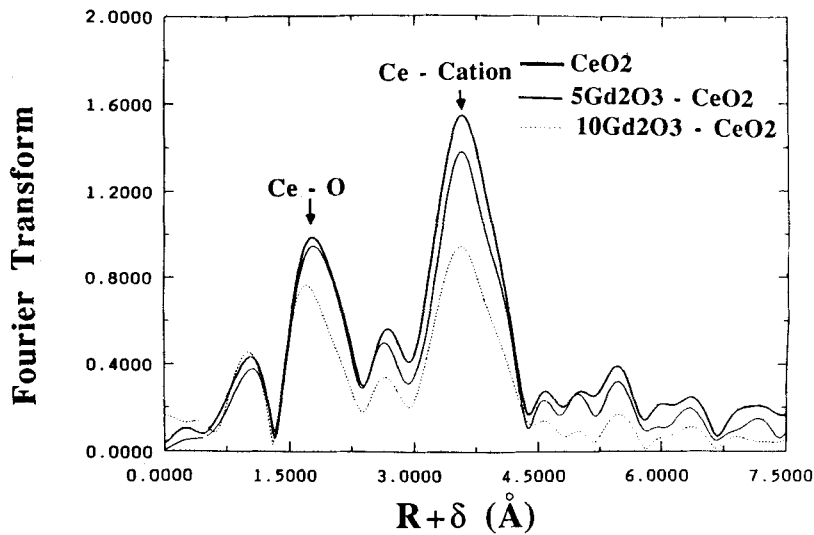

Fig. 9. Comparison of the Fourier transform magnitude for Ce host cation in CeO_2, 5 mol% Gd_2O_3-CeO_2, and 10 mol% Gd_2O_3-CeO_2.

The results of fitting these data using a reference model with 2.34 Å for the Ce–O bond length in CeO_2 are given in Table I. Note that the $\Delta\sigma^2$ values here do not completely reflect the expected distortion due to the high correlation between $\Delta\sigma^2$ and CN. If the CN of Ce^{4+} is fixed at a certain value, e.g. 8, we observe the expected increase in disorder for the doped sample.

IV. Discussion

The XRD and XAS analyses for Sc^{3+} dopant ions suggest that 5 mol% Sc_2O_3 can dissolve completely in ceria prepared by the present experimental method. This amount is much larger than the solubility of Sc_2O_3 in CeO_2 (~1 mol%) reported by Gerhardt et al.[8] The larger metastable solubility may be attributed to our lower processing temperature (850°C vs 1500°C in Ref. 8) and the relatively short firing time which prevents cations from diffusing and partitioning into two phases. From the XAS, the local structures around the dopant cations at this concentration appear to be distinctly different from that of 10-mol%-Sc_2O_3-doped ceria, in which some clustering of defects and dopants seems to have occurred. The most convincing evidence for the Sc^{3+}–Sc^{3+} clustering comes from the contraction of the Sc-cation distance with respect to the reference host lattice. Using this as a criterion, we may regard the defect structure in 5 mol% Sc_2O_3–CeO_2 as a dilute solid solution, consisting of an equal number of Sc_{Ce}–V_O pairs and isolated Sc_{Ce}, and the structure in 10 mol% Sc_2O_3–CeO_2 as a concentrated solid solution, consisting of Sc_{Ce}–V_O–Sc_{Ce} pairs. This picture is consistent with the evidence from XRD.

In the case of Gd_2O_3 doping, the range of dilute solid solutions could be further extended. This is likely because the tendency for forming cation–vacancy–cation clusters decreases with decreasing size misfit of cations,[1] which is quite small in the case of Gd_2O_3–CeO_2 solid solution.

Ordered structures form in concentrated solid solutions and have been extensively studied in the past. A basic feature of these ordered structures in fluorite-type oxides is a highly ordered arrangement of anion vacancies, accompanied by various degrees of cation order.[24] In all cases, the formal anion vacancies are believed to be organized into pairs situated across the body diagonal of the MO_8 cube of the parent fluorite structure. The cation involved thus becomes 6-fold-coordinated in the extreme. The anions of the resultant MO_6 group in turn relax in their positions so as to lie closer to the vertices of a regular octahedron. Our results on 10 mol% Sc_2O_3–CeO_2 and 5 mol% Sc_2O_3–5 mol% Gd_2O_3–CeO_2 are generally compatible with this model.[24]

We have alluded above to the importance of the size (elastic energy) considerations in forming a cation-ordered structure. A clear magnifestation of the strains responsible for elastic interaction is the contraction of the Sc-cation distance observed in the 10-mol%-Sc_2O_3-doped ceria. From the point of view of a CN/ionic size relationship (Pauling's first rule), the cation sites adjacent to oxygen vacancies are more likely to be occupied by the smallest available cations, which favor a lower CN. An extreme example is found in the 5 mol% Sc_2O_3–5 mol% Gd_2O_3–CeO_2 system, in which the smaller Sc^{3+} ions occupy the V_O-associated octahedral sites (Fig. 1(e)) while the larger Gd^{3+} occupy the 8-fold-coordinated sites without any oxygen vacancies (Fig. 1(f)). This is the so-called scavenging effect first suggested by Nowick and co-workers.[1,8]

Such an effect has been previously reported in dilute $ScYO_3$-CeO_2, with evidence for a low symmetry, structural distortion found in relaxation studies.[8] It was explained in terms of a relatively high value of enthalpy of association for the Sc_{Ce}–V_O pairs. An insight into the nature of the distortion was provided by computer simulations by Cormack et al.[25] They suggested that the Sc–O shell in CeO_2 bifurcates into two subshells because of the high polarizability of the CeO_2

matrix which becomes unstable around a severely undersized Sc^{3+} center. In the present study, we have verified this distortion not only in the dilute (5 mol% Sc_2O_3) but also in the concentrated (10 mol% Sc_2O_3) solid solutions. Furthermore, the distortion in the former case occurs even though the pair seems to be constrained by the host matrix so as to maintain the same Sc-cation distance. (The computer simulations found little off-centered Sc displacement but large asymmetric O displacement, which is consistent with our observation of a distortion of the Sc–O bond lengths without a corresponding change in the Sc-cation distance in the dilute solution.) Some discrepancies between these studies, however, should be noted. The Sc–O distances according to our study appear to have shortened in both subshells, whereas the simulation results showed one shortened and the other one lengthened. Despite these details, it seems fairly certain that Sc–O distortion in CeO_2 is now reasonably well established, as is the scavenging effect of unassociated Sc^{3+}.

Models illustrating various configurations of Ce^{4+}, Sc^{3+}, and Gd^{3+} in variously doped CeO_2 solid solutions are summarized in Fig. 1. The further bifurcation of the Sc–O shell which should occur in Figs. 1(c) and (d) is not shown for clarity. It is obvious that the structures of (a) and (f) are similar (8-fold coordination), as are (c) and (d) (7-fold), and, lastly, (b) and (e) (6-fold).

It is interesting to observe that in a scandia-containing system, the concentration where the dilute solid solution crosses over to clustering is between 5 and 10 mol%, corresponding to 9% to 18% of cation substitution. Theoretically, the percolation threshold in three dimensions, around 20%, may be regarded as an upper limit for the range of "dilute" solid solution behavior in which dopant cations are not extensively clustered. On the other hand, the thermodynamic limit is, of course, much lower because of solute defect interactions. The actual limit for "dilute" solid solution behavior in a given metastable solid solution will be between the above two and is determined by diffusion kinetics. The observed crossover in our metastable, supersaturated solid solution of Sc_2O_3–CeO_2 prepared at low temperature is consistent with the above considerations. In this respect, the dopant/defect configurations revealed by studying such systems are presumably similar to those operative in dilute solid solutions and essentially reflect the nature of short-range interactions between dopant cations and the host lattice/defects. However, they could be significantly different from the equilibrium configurations in the concentrated solid solutions which are more dictated by long-range interactions and cooperative relaxations.

Finally, our results can be interpreted as indicating a clustering tendency for Sc^{3+} cations and oxygen vacancies to form a Sc_2O_3-like structure, which increases in the following order: 5 mol% Sc_2O_3–CeO_2, 10 mol% Sc_2O_3–CeO_2, and 5 mol% Sc_2O_3–5 mol% Gd_2O_3–CeO_2. This points to an interesting possibility that the formation of a second phase may indeed be catalyzed by the presence of a third type of cation which supplies the necessary oxygen vacancies at the forming stage of the new structure without participating in the new phase itself. Future research along this line may prove illuminating to the field of phase transformation.

V. Conclusions

X-ray absorption measurements (EXAFS and XANES) are reported for ceria doped with the trivalent cations Sc^{3+} (severely undersized) and Gd^{3+} (slightly oversized), for both singly and doubly doped samples. Major findings are the following:

(1) Sc_2O_3 (5 mol%) can dissolve completely in ceria to form a ceria solid solution when the processing temperatures are kept low. The dopant cation sublattice is completely random and is constrained by the host cation sublattice. This composition is believed to be representative of a dilute solid solution.

(2) Defect clustering between oxygen vacancies and Sc^{3+} ion occurs in 10-mol%-Sc_2O_3-doped ceria, as evidenced by the contraction of the lattice parameter and the Sc^{3+}-cation distance. This composition is believed to be representative of a concentrated solid solution.

(3) A distortion of the oxygen-coordinated polyhedron around an undersized Sc^{3+} into two subshells has been observed in both of the above compositions.

(4) An octahedrally coordinated Sc-ordered structure forms in 5 mol% Sc_2O_3–5 mol% Gd_2O_3–CeO_2 because of the strong scavenging effect of Sc^{3+} ions on oxygen vacancies induced by Gd^{3+} ions. The Gd^{3+} cations are randomly distributed and are located at the centers of oxygen cubes.

(5) Gd^{3+} dopant cations substitute for Ce^{4+} ions and are distributed randomly in both 5 mol% and 10 mol% Gd_2O_3–CeO_2.

References

[1]A.S. Nowick, *Diffusion in Crystalline Solids;* Ch. 3. Edited by G.E. Murch and A.S. Nowick. Academic Press, Orlando, FL, 1984.

[2]R. Gerhardt-Anderson and A.S. Nowick, "Ionic Conductivity of CeO_2 with Trivalent Dopants of Different Ionic Radii," *Solid State Ionics,* **5**, 547–50 (1981).

[3]D.Y. Wang and A.S. Nowick, "Dielectric Relaxation in Yttria-Doped Ceria Solid Solutions," *J. Phys. Chem. Solids,* **44**, 639 (1983).

[4]A.S. Nowick, D.Y. Wang, D.S. Park, and J. Griffith, "Oxygen-Ion Conductivity and Defect Structure of CeO_2"; pp. 673–77 in *Fast Ion Transport in Solids.* Edited by P. Vashishta, J.N. Mundy, and G.K. Shenoy. North-Holland, Amsterdam, Netherlands, 1979.

[5]D.K. Hohnke, "Ionic Conductivity in Doped Oxides with the Fluorite Structure," *Solid State Ionics,* **5**, 531–34 (1981).

[6]R. Gerhardt, W.-K. Lee, and A.S. Nowick, "Anelastic and Dielectric Relaxation of Scandia-Doped Ceria," *J. Phys. Chem. Solids,* **48**, 563–69 (1987).

[7]D.Y. Wang and A.S. Nowick, "Dielectric Relaxation from a Network of Charged Defects in Dilute CeO_2:Y_2O_3 Solid Solutions," *Solid State Ionics,* **5**, 551–54 (1981).

[8]R. Gerhardt, F. Zamani-Noor, A.S. Nowick, C.R.A. Catlow, and A.N. Cormack, "Study of Sc_2O_3-Doped Ceria by Anelastic Relaxation," *Solid State Ionics,* **9–10**, 931–36 (1983).

[9]R.J. Tesch, C.D. Wirkus, and M.F. Berard, "Self-Diffusion of Er and Hf in Polycrystalline Er_2O_3-Stabilized HfO_2," *J. Am. Ceram. Soc.,* **65**, 511–15 (1982).

[10]T. Kudo and H. Obayashi, "Oxygen Ion Conduction of the Fluorite-Type $Ce_{1-x}Ln_xO_{2-x/2}$ (Ln = Lanthanoid Element)," *J. Electrochem. Soc.,* **122**, 142 (1975).

[11]D.W. Strickler and W.G. Carlson, "Electrical Conductivity in the ZrO_2-Rich Region of Several M_2O_3-ZrO_2 Systems," *J. Am. Ceram. Soc.,* **48**, 286–88 (1965).

[12]J.G. Allpress and H.J. Rossell, "A Microdomain Description of Defective Fluorite-Type Phase $Ca_xM_{1-x}O_{2-x}$ (M = Zr, Hf; x = 0.1–0.2)," *J. Solid State Chem.,* **15**, 68–78 (1975).

[13]T. Moriga, A. Yoshiasa, F. Kanamaru, and K. Koto, "Crystal Structure Analysis of the Pyrochlore- and Fluorite-type $Zr_2Gd_2O_7$ and Anti-phase Domain Structure," *Solid State Ionics,* **31**, 319–28 (1989).

[14]M.R. Thornber and D.J.M. Bevan, "Mixed Oxides of the Type MO_2 (Fluorite)—M_2O_3, III. Crystal Structures of the Intermediate Phases $Zr_5Sc_2O_{13}$ and $Zr_3Sc_4O_{12}$," *Acta Crystallogr.,* **B24**, 1183 (1968).

[15]G.P. Williams, "Electron Binding Energies"; pp. 2–5 in *X-Ray Data Booklet.* Lawrence Berkeley Laboratory, University of California, Berkeley, CA, 1986.

[16]B.K. Teo, *EXAFS: Basic Principles and Data Analysis;* p. 131. Springer-Verlag, Berlin, FRG, 1984.

[17]O. Knop and J.M. Hartley, "Refinement of the Crystal Structure of Scandium Oxide," *Can. J. Chem.,* **46**, 1446–50 (1968).

[18]G.S. Waldo and J.E. Penner-Hahn; unpublished work.

[19]R.D. Shannon, "Revised Effective Ionic Radii and Systematic Studies of Interatomic Distances in Halides and Chalcogenides," *Acta Crystallogr.,* **A32**, 751–67 (1976).

[20]A.F. Wells, *Structural Inorganic Chemistry;* p. 545. Oxford University Press, Oxford, U.K., 1984.

[21]R.A. Scott, "Measurement of Metal–Ligand Distances by EXAFS," *Methods Enzymol.,* **177**, 414–59 (1985).

[22]C.R.A. Catlow, A.V. Chadwick, G.N. Greaves, and L.M. Moroney, "EXAFS Study of Yttria-Stabilized Zirconia," *J. Am. Ceram. Soc.,* **69**, 272–77 (1986).

[23]J.C.J. Bart, "Near-Edge X-ray Absorption Spectroscopy in Catalysis," *Adv. Catal.,* **34**, 203–97 (1986).

[24]H.J. Rossell, "Ordering in Anion-Deficient Fluorite-Related Oxides," *Adv. Ceram.,* **3**, 47–63 (1981).

[25]A.N. Cormack, C.R.A. Catlow, and A.S. Nowick, "Theoretical Studies of Off-Centre Sc^{3+} Impurities in CeO_2," *J. Phys. Chem. Solids,* **50**, 177–81 (1989).

□